Article

Not peer-reviewed version

Design of a Novel Multiepitope Vaccine against Glioblastoma by In-Silico Approaches

Sako Mirzaie , Kevin Da Yuan , Heyu Ni , Xiao Yu Wu *

Posted Date: 29 August 2024

doi: 10.20944/preprints202408.2058.v1

Keywords: Glioblastoma; vaccine; urokinase plasminogen activator surface receptor; Integrin beta-3; HLA class I

 doi:10.20944/preprints202408.2058.v1

Article

Design of a Novel Multiepitope Vaccine Against Glioblastoma by In-Silico Approaches

Sako Mirzaie [1,*], Kevin Da Yuan [1], Heyu Ni [2,3,4] and Xiao Yu Wu [1,*]

[1] Advanced Pharmaceutics and Drug Delivery Laboratory, Leslie Dan Faculty of Pharmacy, University of Toronto, Toronto, ON, M5S 3M2, Canada; s.mirzaie@utoronto.ca
[2] Department of Laboratory Medicine and Pathobiology, University of Toronto, ON, Canada
[3] Keenan Research Centre for Biomedical Science, St. Michael's Hospital, Toronto Canada
[4] Canadian Blood Services Centre for Innovation, Toronto, ON, Canada
* Correspondence: sxy.wu@utoronto.ca; s.mirzaie@mail.utoronto.ca

Simple Summary: Glioblastoma (GBM) stands as the most prevalent malignant primary brain tumor, accounting for approximately 57% of all gliomas and 48% of all primary malignant central nervous system tumors. In recent years, substantial progress has been made in multimodal treatments for GBM using a combination of surgery, radiotherapy, systemic therapies such as chemotherapy, and comprehensive supportive care. Despite this, the overall outlook for patients remains bleak, with long-term survival being an uncommon occurrence. Our study aimed to develop a novel peptide-based vaccine using advanced molecular modeling and immuno-informatics techniques to combat GBM. This vaccine holds the potential to revolutionize GBM treatment and improve patient outcomes.

Abstract: Glioblastoma (GBM) is the most common malignant primary brain tumor; with a median survival rate of less than two years. Currently, there is no cure for GBM, underscoring the urgent need for innovative treatment approaches. Vaccine design emerges as a crucial strategy, offering a safe and effective means for both preventive and therapeutic interventions against GBM. In this study, we targeted four GBM-associated mutated surface proteins—urokinase plasminogen activator surface receptor (PLAUR), integrin beta-3 (ITGB3), and the B-41 alpha chain (HLA-B) and A-24 alpha chain (HLA-A) of the HLA class I histocompatibility antigens—to design a peptide-based vaccine. The vaccine construct includes cytotoxic T lymphocyte (CTL) and T helper cell (Th cell) epitopes, and was meticulously evaluated for antigenicity, allergenicity, and toxicity. The results indicate that the vaccine is antigenic and non-allergenic, making it a promising candidate. Additionally, the physico-chemical properties of the vaccine suggest stability and suitability for further development. Immune simulation studies predict efficient immune responses upon vaccine administration. Our vaccine shows promise as a potential tool in the fight against GBM, offering new hope for patients facing this devastating disease

Keywords: glioblastoma; vaccine; urokinase plasminogen activator surface receptor; integrin beta-3; HLA class I

1. Introduction

Glioblastoma multiforme (GBM) is the most common and the most aggressive primary brain tumor in adults [1]. As the most prevalent high-grade glioma, GBM occurs in 3.22 people per 100,000 population [2]. This incidence escalates notably beyond the age of 54, reaching a peak rate of 15.24 per 100,000 population in individuals aged 75 to 84 [3]. Despite its prevalence, the etiology of GBM remains largely elusive for the majority of affected patients. A minority, comprising less than 5% of cases, exhibits a genetic alteration rendering them more susceptible to various tumor types, GBM included. Furthermore, a mere fraction—less than 20% of GBM patients possess a significant familial history of cancer. Although exposure to ionizing radiation unequivocally stands as a confirmed cause of GBM, it accounts for only a minor fraction of cranial tumors ultimately diagnosed as GBMs. Other

 doi:10.20944/preprints202408.2058.v1

conceivable contributors, such as cell phone exposure, viral factors including cytomegalovirus, and genetic predispositions, are presently subjects of investigation, yet their roles as definitive causal elements remain unestablished. Early detection of GBM remains a challenge, with standard magnetic resonance imaging standing as the foremost method for initial identification. Regrettably, by the time a discernible GBM lesion manifests in imaging, the tumor has already progressed to an advanced stage [4].

GBM displays distinctive attributes including extensively necrotic, hypoxic, and actively proliferating regions, characteristics commonly observed in high-grade tumors [5]. The prevailing standard of care entails tumor reduction pursued by chemo-radiotherapy, yielding an average survival period of approximately 14.5 months for patients [6]. Nevertheless, novel clinical approaches have hitherto shown limited success in augmenting the survival rates of GBM patients [7]. Notably, immunotherapeutic methodologies, including those involving dendritic cells (DCs) or targeting the Programmed Cell Death protein-1 (PD-1) immune checkpoint within GBM, have been introduced. Nonetheless, their effectiveness awaits confirmation through human clinical trials [8,9].

The development of a preventative or therapeutic vaccine offers a hope to combat GBM. Extensive research on both human and animal models has demonstrated that immunity against GBM is correlated with responses from CD4+ T helper cell (Th cell), CD8+ cytolytic T lymphocytes (CTLs), and mechanisms involving antibody-dependent cellular cytotoxicity [10,11]. The cytokines IFN-α, IFN-β, IFN-γ, IL-12, and IL-13 have been identified as essential factors for conferring protection against GBM or hindering the growth of human GBM cells [12]. Demonstrative evidence has established that IL-4 exerts an inhibitory effect on GBM xenograft growth, observable both in inducible IL-4 KO cell lines [13] and through subcutaneous administration or retroviral delivery [14]. Conversely, the cytokines IL-8 and IL-10 are implicated in promoting tumor advancement, angiogenesis, and invasiveness [15]. Additionally, toll-like receptor 4 (TLR-4) has been implicated in orchestrating immune protective responses [16].

This study focused on the in-silico development of a potential peptide-based vaccine candidate for GBM, utilizing immuno-informatics analyses and molecular dynamics (MD) simulations. In the realm of GBM vaccines, two prominent targets have emerged: epidermal growth factor receptor variant III (EGFRvIII) [17] and mutant isocitrate dehydrogenase 1 (IDH1) [18]. Owing to the recently found lack of survival benefit of a peptide vaccine targeting EGFRvIII (Rindopepimut) in the ACT IV randomized phase III trial [19], the interests have shifted to IDH1 as the preferred focal point for GBM vaccine development. However, it is important to note that IDH1 functions as an intracellular enzyme, which could potentially influence the efficacy of the vaccine. Proteomics analysis revealed that among the 114 mutations unique to GBM, four are found in extracellular proteins: urokinase plasminogen activator surface receptor (PLAUR), Integrin beta-3 (ITGB3), and discrete subunits of the HLA class I histocompatibility antigens; the B-41 alpha chain (HLA-B) and A-24 alpha chain (HLA-A) [20]. Of these proteins, PLAUR is an attractive target for the treatment of cancer, as it is expressed at low levels in healthy tissues but at high levels in malignant tumours [21]. In addition, it is closely related to the invasion and metastasis of malignant tumours, plays important roles in the degradation of extracellular matrix (ECM), tumour angiogenesis, cell proliferation and apoptosis, and is related to the multidrug resistance (MDR) of tumour cells, which has vital guiding significance for the evaluation of tumor malignancy and prognosis [21]. On the other hand, ITGB3 expression correlates with high-grade GBM [22]. Similarly, it has been demonstrated that the HLA-A [23] and HLA-B [20] alleles are common among glioma patients. Taking these contexts into consideration, we have utilized the mutated segments of these four targets as the basis for constructing the vaccine.

2. Materials and Methods

2.1. Target Selection and Epitope Screening

In the initial phase of this study, we extracted the wild-type amino acid sequences of four surface proteins—PLAUR (Q03405), ITGB3 (P05106), HLA-B (P01889), and HLA-A (P04439)—from the Uniprot database in FASTA format [24]. For constructing the mutants, the residues Arg, Asn, Thr,

 doi:10.20944/preprints202408.2058.v1

and Ile were substituted by His, Asp, Lys, and Thr in PLAUR, ITGB3, HLA-B, and HLA-A, respectively [20]. All potential Cytotoxic T lymphocytes (CTL) and T helper cell (Th cell) epitopes capable of binding to MHC class II molecules were identified at their respective mutation sites (Figure 1). The expression levels and survival probabilities of HLA-B, PLAUR, HLA-A, and ITGB3 in both healthy individuals and GBM patients were determined using the ULCAN database [25]. Given the extensive number of epitopes, they were screened for antigenicity, toxicity, and allergenicity to select the most suitable ones. The VaxiJen v2.0 server (http://www.ddg-pharmfac.net/vaxijen/VaxiJen/VaxiJen.html) was employed to forecast the epitopes' antigenicity [26]. The VaxiJen v2.0 server can compute the antigenicity of a wide range of microorganisms, including bacteria, viruses, tumors, parasites, and fungi. The prediction accuracy of the VaxiJen v2.0 server ranges from 70% to 89%. For this analysis, the tumor was chosen as the target organism, with the antigenicity threshold established at 0.5.

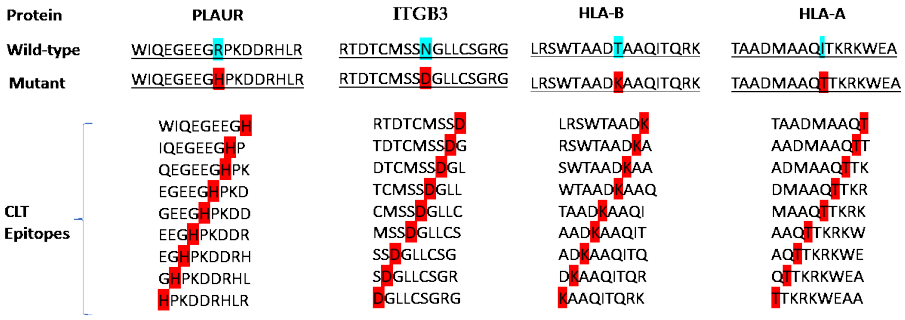

Figure 1. The wild-type, mutant and CTL epitopes of PLAUR, ITGB3, HLA-B and HLA-A. The wild-type and point mutations are highlighted in cyan and red, respectively. .

The AllerTOP v. 2.0 server (https://www.ddg-pharmfac.net/AllerTOP/method.html) was employed to evaluate the allergenicity of the epitopes [27]. In addition, The approach employed by this server hinges on the auto cross covariance (ACC) transformation of amino acid sequences into standard vectors of consistent length [28]. Furthermore, IL4pred (https://webs.iiitd.edu.in/raghava/il4pred/design.php) was employed to predict IL-4 inducing epitopes, while IFNepitope (https://webs.iiitd.edu.in/raghava/ifnepitope/design.php) was used for predicting IFN-γ inducing epitopes. For predicting IL-4 inducing epitopes, the SVM-based model with a threshold of 0.2 was chosen [29]. Meanwhile, for IFN-γ inducing epitopes, an SVM-based model combined with the IFN-gamma versus other cytokine models was selected [30].

2.2. Assembly of the Multi-Epitope Vaccine

Epitopes identified in the prior step were employed to assemble a multi-epitope vaccine. For the CTL epitopes, AAY linkers were utilized. By inserting linkers, the representation and proper separation of the epitopes will be improved. Additionally, the 50S ribosomal protein L7/L12 (Locus RL7_MYCTU) with the accession number P9WHE3 was chosen as an adjuvant to boost the immunogenicity of the vaccine candidate. Its amino acid sequence was connected to the N-terminus of the chimeric sequences using an EAAAK linker.

2.3. Assessment of the Vaccine's Antigenicity, Allergenicity, and Physicochemical Characteristics

Evaluating antigenicity is crucial in the vaccine design process. We utilized two servers, VaxiJen v2.0 and ANTIGENpro, to forecast the antigenic tendencies of the final vaccine construct. ANTIGENpro (http://scratch.proteomics.ics.uci.edu/) predicts protein antigenicity by employing five machine learning methodologies and various representations of the primary sequence [31]. To confirm the non-allergenic nature of the vaccine, we utilized AllerTOP v. 2.0 for allergenicity predictions. In addition, the Expasy ProtParam server (https://web.expasy.org/protparam/) was employed to anticipate different physicochemical attributes of the multi-epitope vaccine, such as

 doi:10.20944/preprints202408.2058.v1

amino acid composition, theoretical pI, molecular weight, instability index, half-life, aliphatic index, and the grand average of hydropathicity (GRAVY) [32].

2.4. Secondary Structure Prediction

The Prabi server (https://npsa-prabi.ibcp.fr/cgi-bin/npsa_automat.pl?page=/NPSA/npsa_gor4.html) was employed to estimate the proportion of secondary structure elements in the vaccine construct. The server utilizes the GOR IV prediction method, which boasts an average accuracy rate of 64.4% [33].

2.5.3. D Structure Modeling, Refinement, and Verification of the Multi-Epitope Vaccine

The 3D structure of the multi-epitope vaccine was predicted using the I-TASSER server (https://zhanglab.ccmb.med.umich.edu/I-TASSER/). This server predicts three-dimensional structures from the amino acid sequence by piecing together segments from threading templates and provides a C-score to gauge the precision of the generated models [34]. The quality of the models were assessed by using the ProTSAVv server [35]. ProTSAV is a validated server, tested on approximately 64,446 protein structures. These encompass experimental structures from RCSB, predicted model structures for CASP targets, and those from public decoy sets. For experimentally solved structures, ProTSAV boasts a specificity of 100% and a sensitivity of 98%. For predicted protein structures of CASP11 targets under 2 Å, it achieves a specificity of 88% and a sensitivity of 91%. By integrating multiple methodologies, the server addresses the constraints inherent to individual servers or methods, proving to be a robust tool for quality assessment [35]. The selected model from the previous step was refined by using GalaxyRefine2 web server [36].

2.6. B-cell Epitopes Prediction

B lymphocytes are pivotal components of the immune system, responsible for antibody production, thereby fostering long-term immunity [37].

Linear B-cell epitopes were forecasted using the BCPREDS server (https://webs.iiitd.edu.in/raghava/bcepred/bcepred_submission.html) [38]. This server employs a subsequence kernel-based SVM classifier and boasts an accuracy of 74.57% in predicting linear B-cell epitopes [39]. Additionally, the ElliPro server (http://tools.iedb.org/ellipro/) was engaged for discontinuous B-cell epitope predictions. ElliPro implements residue clustering algorithms, combined with Tornton's method, to predict these epitopes. Each predicted epitope is given a score, termed the PI (protrusion index) value [40].

2.7. Molecular Docking and MD Simulations

The CTL epitopes that successfully passed the screening phase were subjected to molecular docking against MHC class I (HLA A1, HLA A2, and HLA A3). HyperChem 8 was used for constructing the epitopes structures [41]. Autodock vina [42] with its default setting was engaged to dock the epitopes with the MHC molecules. After assembling the epitopes, incorporating the adjuvant, and constructing the vaccine, a 500 ns MD simulation was conducted to refine the structure and eliminate steric clashes. Subsequently, the final snapshot of the vaccine was retained for additional modeling analyses. To explore the potential interaction between the vaccine construct and TLR4 (PDB ID: 4G8A) [43], the ClusPro 2.0 server (https://cluspro.org/login.php) was utilized [44]. After 500 ns MD simulation for relaxing the vaccine construct, a 200 ns MD simulation was conducted for the vaccine: TLR4 complex.

All MD simulations were done by Desmond simulation package from Schrödinger Inc [45]. During each MD run, parameters of 310 K temperature and 1 bar pressure were maintained. For the simulation, the OPLS3 (Optimized Potentials for Liquid Simulations version 3) force field parameters was used [46]. The long-range electrostatic interactions were computed using the particle mesh Ewald method [47], with a cutoff radius of 9.0 Å for Coulomb interactions. The system was solvated using the explicit TIP3P (three-site transferrable intermolecular potential) water model within an

 doi:10.20944/preprints202408.2058.v1

cubic periodic box that maintained periodic boundary conditions [48]. Na^+ and Cl^- were added as the counter ions, ensuring system neutrality. A distance of 10.0 Å was maintained between the periodic boundary conditions and the nearest vaccine: TLR4 complex atoms. The Martyna–Tuckerman–Klein chain coupling scheme [49] managed pressure, while the Nosé–Hoover chain coupling scheme [50] oversaw temperature during MD runs. Trajectory data were recorded every 10 ps. Analysis of the MD outputs were conducted using Visual Molecular Dynamics (VMD) [51], alongside the Simulation Quality Analysis and Simulation Interaction Diagram tools within the Desmond MD package.

2.8. Analysis of the Immune Profile for the Multi-Epitope Vaccine Construct

For an effective immune response against cancer cells, it's crucial to understand the immune characteristics of the constructed vaccine through an immune simulation method. Thus, we assessed the immune profile of the final multi-epitope vaccine by inputting the vaccine construct sequence into the C-ImmSim 10.1 web server [52]. C-ImmSim operates on the principles encompassing several specific elements of the immune system. These include antigen processing and presentation to CTL and Th cell, intercellular cooperation, B-cell and T-cell maturation, memory cell formation, clonal selection based on antigen affinity, the theory of clonal deletion, antibody hypermutation, T-cell replicative senescence, and anergy in both B and T lymphocytes, among others.

3. Results

3.1. Target Selection and Preliminary Analysis

An ideal vaccine candidate should be prominently displayed on the surface, highly produced, and broadly distributed. In our research, we chose four cell surface proteins identified as GBM-associated antigens. These proteins should exhibit high expression in GBM, possess significant immunogenicity, and be surface-exposed. The gene expression profile of the target proteins was studied by using TCGA database which exhibited significant over expression in GBM samples in comparison to normal tissue (Figures S1A, S1C, S1E, and S1G). We further explored the association of the selected proteins with the survival in GBM patients. For this, the survival analysis of the GBM patient was accomplished using the clinical data present in the TCGA database and the results are shown in Figures S1B, S1D, S1F, and S1H. These figures demonstrate that as the gene expression of these proteins increases, there's a corresponding decrease in survival probability for patients.

The amino acid sequences for four proteins were retrieved from the Uniprot database to design a construct of a multi-epitope vaccine candidate against GBM. Subsequently, the mutated segments of each sequence were used to formulate a total of 36 CTL epitopes, as depicted in Figure 1. For the Th cell epitopes, those that could bind to the MHC class II supertypes were chosen for subsequent analysis, resulting in a total of 14 Th cell epitopes. CTL epitopes were then evaluated for antigenicity, allergenicity, toxicity, IFN-γ –inducing, and IL-4- inducing using VaxiJen v2.0, AllerTOP v. 2.0, ToxinPred, IFNepitope, and IL4pred servers, respectively (Table 1). The same screening process was applied to Th cell epitopes, as summarized in Table 2. By evaluating the data presented in both Table 1 and Table 2, we identified four epitopes for inclusion in the final vaccine: "AQTTKRKWE" (designated as epitope C1), "QTTKRKWEA" (epitope C2), "TTKRKWEAA" (epitope C3), and "DMAAQTTKRKWEAAH" (epitope H1). Furthermore, we conducted molecular docking studies to examine the interaction mode and affinity of each epitope with HLA-A1, HLA-A2, and HLA-A3 as illustrated in Figures S2 to S10.

Table 1. Predicted CTL epitopes of PLAUR, ITGB3, HLA-B and HLA-A proteins.

Protein	Epitopes	VaxiJen	Allergenicity	Toxicity	IFN-γ – inducing	IL-4-inducing	Final decision
PLAUR	WIQEGEEGH	1.1681 (Probable Antigen)	Probable Non-Allergen	Non-Toxin	Positive	Non-IL4-inducer	-

 doi:10.20944/preprints202408.2058.v1

	IQEGEEGHP	1.4977 (Probable Antigen)	Probable Non-Allergen	Non-Toxin	Positive	Non-IL4-inducer	-
	QEGEEGHPK	1.3359 (Probable Antigen)	Probable Allergen	Non-Toxin	Positive	IL4-inducer	-
	EGEEGHPKD	1.1271 (Probable Antigen)	Probable Allergen	Non-Toxin	Positive	IL4-inducer	-
	GEEGHPKDD	0.8220 (Probable Antigen)	Probable Allergen	Non-Toxin	Positive	Non-IL4-inducer	-
	EEGHPKDDR	0.2950 (Probable Non-Antigen)	Probable Allergen	Non-Toxin	Positive	Non-IL4-inducer	-
	EGHPKDDRH	-0.1423 (Probable Non-Antigen)	Probable Allergen	Non-Toxin	Positive	Non-IL4-inducer	-
	GHPKDDRHL	-0.1795 (Probable Non-Antigen)	Probable Allergen	Non-Toxin	Negative	Non-IL4-inducer	-
	HPKDDRHLR	-0.4382 (Probable Non-Antigen)	Probable Allergen	Non-Toxin	Negative	IL4-inducer	-
	RTDTCMSSD	0.0279 (Probable Non-Antigen)	Probable Allergen	Non-Toxin	Negative	IL4-inducer	-
	TDTCMSSDG	0.1181 (Probable Non-Antigen)	Probable Allergen	Non-Toxin	Negative	IL4-inducer	-
	DTCMSSDGL	-0.1421 (Probable Non-Antigen)	Probable Allergen	Non-Toxin	Negative	IL4-inducer	-
ITGB3	TCMSSDGLL	-0.0823 (Probable Non-Antigen)	Probable Allergen	Non-Toxin	Positive	IL4-inducer	-
	CMSSDGLLC	-0.3962 (Probable Non-Antigen)	Probable Allergen	Non-Toxin	Negative	IL4-inducer	-
	MSSDGLLCS	-0.0032 (Probable Non-Antigen)	Probable Allergen	Non-Toxin	Positive	IL4-inducer	-
	SSDGLLCSG	0.0546 (Probable Non-Antigen)	Probable Allergen	Non-Toxin	Negative	IL4-inducer	-
	SDGLLCSGR	-0.0087 (Probable Non-Antigen)	Probable Allergen	Non-Toxin	Negative	Non-IL4-inducer	-
	DGLLCSGRG	0.4925 (Probable Non-Antigen)	Probable Non-Allergen	Non-Toxin	Negative	Non-IL4-inducer	-
	LRSWTAADK	0.0708 (Probable Non-Antigen)	Probable Non-Allergen	Non-Toxin	Negative	IL4-inducer	-
	RSWTAADKA	0.1046 (Probable Non-Antigen)	Probable Non-Allergen	Non-Toxin	Positive	Non-IL4-inducer	-
	SWTAADKAA	0.1046 (Probable Non-Antigen)	Probable Allergen	Non-Toxin	Positive	Non-IL4-inducer	-
	WTAADKAAQ	0.5204 (Probable Antigen)	Probable Allergen	Non-Toxin	Positive	Non-IL4-inducer	-
HLA-B	TAADKAAQI	1.5233 (Probable Antigen)	Probable Allergen	Non-Toxin	Negative	Non-IL4-inducer	-

 doi:10.20944/preprints202408.2058.v1

	AADKAAQIT	1.5395 (Probable Antigen)	Probable Allergen	Non-Toxin	Positive	Non-IL4-inducer	-
	ADKAAQITQ	1.6355 (Probable Antigen)	Probable Allergen	Non-Toxin	Negative	Non-IL4-inducer	-
	DKAAQITQR	1.6396 (Probable Antigen)	Probable Non-Allergen	Non-Toxin	Positive	Non-IL4-inducer	-
	KAAQITQRK	1.2152 (Probable Antigen)	Probable Non-Allergen	Non-Toxin	Negative	Non-IL4-inducer	-
	TAADMAAQT	0.6747 (Probable Antigen)	Probable Non-Allergen	Non-Toxin	Negative	IL4-inducer	-
	AADMAAQTT	0.6145 (Probable Antigen)	Probable Non-Allergen	Non-Toxin	Negative	IL4-inducer	-
	ADMAAQTTK	0.8434 (Probable Antigen)	Probable Allergen	Non-Toxin	Negative	IL4-inducer	-
	DMAAQTTKR	1.0065 (Probable Antigen)	Probable Non-Allergen	Non-Toxin	Negative	IL4-inducer	-
	MAAQTTKRK	1.0223 (Probable Antigen)	Probable Non-Allergen	Non-Toxin	Negative	Non-IL4-inducer	-
	AAQTTKRKW	0.5899 (Probable Antigen)	Probable Non-Allergen	Non-Toxin	Negative	Non-IL4-inducer	-
HLA-A	AQTTKRKWE (C1)	0.7411 (Probable Antigen)	Probable Non-Allergen	Non-Toxin	Positive	IL4-inducer	*
	QTTKRKWEA (C2)	0.6981 (Probable Antigen)	Probable Non-Allergen	Non-Toxin	Positive	IL4-inducer	*
	TTKRKWEAA (C3)	0.5519 (Probable Antigen)	Probable Non-Allergen	Non-Toxin	Positive	IL4-inducer	*

Table 2. Predicted Th cell epitopes of PLAUR, ITGB3, HLA-B and HLA-A proteins.

Protein	Epitopes	VaxiJen	Allergenicity	Toxicity	IFN-γ – inducing	IL-4-inducing	Final decision
	ADMAAQTTKRKWEAA	0.6847 (Probable Antigen)	Probable Non-Allergen	Non-Toxin	Negative	IL4-inducer	-
	AADMAAQTTKRKWEA	0.6458 (Probable Antigen)	Probable Non-Allergen	Non-Toxin	Negative	IL4-inducer	-
HLA-A	DMAAQTTKRKWEAAH	0.6882 (Probable Antigen)	Probable Non-Allergen	Non-Toxin	Positive	IL4-inducer	-
	TAADMAAQTTKRKWE	0.6752 (Probable Antigen)	Probable Non-Allergen	Non-Toxin	Negative	IL4-inducer	-
	MAAQTTKRKWEAAHE	0.6191 (Probable Antigen)	Probable Non-Allergen	Non-Toxin	Positive	Non-IL4-inducer	-

 doi:10.20944/preprints202408.2058.v1

	ADMAAQTTKRKWEAA	0.6847 (Probable Antigen)	Probable Non-Allergen	Non-Toxin	Negative	IL4-inducer	-
	AADMAAQTTKRKWEA	0.6458 (Probable Antigen)	Probable Non-Allergen	Non-Toxin	Negative	IL4-inducer	-
	DMAAQTTKRKWEAAH (H1)	0.6882 (Probable Antigen)	Probable Non-Allergen	Non-Toxin	Positive	IL4-inducer	*
	TAADMAAQTTKRKWE	0.6752 (Probable Antigen)	Probable Non-Allergen	Non-Toxin	Negative	IL4-inducer	-
	WTAADMAAQTTKRKW	0.4225 (Probable Non-Antigen)	Probable Non-Allergen	Non-Toxin	Negative	Non-IL4-inducer	-
	MAAQTTKRKWEAAHE	0.6191 (Probable Antigen)	Probable Non-Allergen	Non-Toxin	Positive	Non-IL4-inducer	-
	DGLLCSGRGKCECGS	0.8628 (Probable Antigen)	Probable Non-Allergen	Toxin	Negative	Non-IL4-inducer	-
ITGB3	SDGLLCSGRGKCECG	0.5730 (Probable Antigen))	Probable Non-Allergen	Toxin	Negative	Non-IL4-inducer	-
	SSDGLLCSGRGKCEC	0.7534 (Probable Antigen)	Probable Non-Allergen	Toxin	Negative	Non-IL4-inducer	-

The molecular docking analysis demonstrated that the docking energies for various epitopes ranged from -9.9 to -11.28 kcal/mol, indicating a high affinity between the epitopes and their respective binding sites in MHC molecules.

3.2. Constructing the Vaccine

To construct the multi-epitope vaccine, we merged three CTL (C1, C2, and C3) epitopes and one Th cell (H1) epitope, connecting them using AAY linkers. This fusion process generated a sequence comprising 51 amino acids. To enhance the vaccine's effectiveness, an adjuvant sequence, consisting of 130 amino acids (MAKLSTDELLDAFKEMTLLELSDFVKKFEETFEVTAAAPVAVAAAGAAPAGAAVE-AAEEQSEFDVILEAAGDKKIGVIKVVREIVSGLGLKEAKDLVDGAPKPLLEKVAKE-AADEAKAKLEAAGATVTVK), was appended to the N-terminal of the vaccine sequence, facilitated by an EAAAK linker. Consequently, the final vaccine construct, designed with improved efficacy, encompassed a total of 186 amino acids (Figure 2A).

3.3. Antigenicity, Allergenicity, and Physico-Chemical Properties Assessment

The antigenicity of the RVC sequence was estimated using the VaxiJen 2.0 server and followed by ANTIGENpro. The overall prediction for the constructed vaccine was performed by using VaxiJen 2.0 server was 0.6314 with a tumor model at a threshold of 0.5. Likewise, the overall prediction of antigenicity probability was 0.9399 performed by the ANTIGENpro server. The AllerTOP v. 2.0 server was utilized to forecast the allergic potential of the suggested vaccine, and the results suggested that it did not possess allergenic properties. The predicted molecular weight (MW) and theoretical isoelectric point value (pI) of the final vaccine were 19.88 kDa and 5.7, respectively. According to the PI parameter, the vaccine is predicted naturally acidic. The estimated half-life was 30 h in mammalian reticulocytes in vitro, more than 20 h in yeast, and over 10 h in E. coli in vivo. The vaccine was indicated to be considered thermally stable, as represented by instability indexes of 24.96 [53]. The aliphatic index of the vaccine was 81.67, and its GRAVY score was reported to be -0.242.

 doi:10.20944/preprints202408.2058.v1

3.4. Secondary Structure Prediction, Tertiary Structure Modeling, Refinement, and Validation

The secondary structure composition of the multi-epitope vaccine was determined using the Prabi server. The analysis revealed the presence of alpha-helix (79.03%), extended strand (7.53%), and random coil (13.44%) components, as depicted in Figure 2B. The five models of the 3D structure of the vaccine construct were generated by the I-TASSER server using the threading templates (PDB Hit: 1dd3A, 2ftcF, 1rqvA, 2ongA, 3n0fA, 7cjyA, 3m02A, 6o9pA, 3rkoM, and 1n1zA). The computed C-score values for models 1–5 were − -2.72, -2.74, -2.89, -3.35, and -3.69, respectively. The C-score is usually within the range of − 5 to 2, where a higher C-score for the model demonstrates that it has a high level of confidence [34]. In the next step, the quality of each generated model was tested by ProTSAV server (Figures 3A-E). Based on ProTSAV overall score, model 2 was chosen for further refinement by GalaxyRefine2 web server and its ProTSAV overall score was assessed again (Figure 3F).

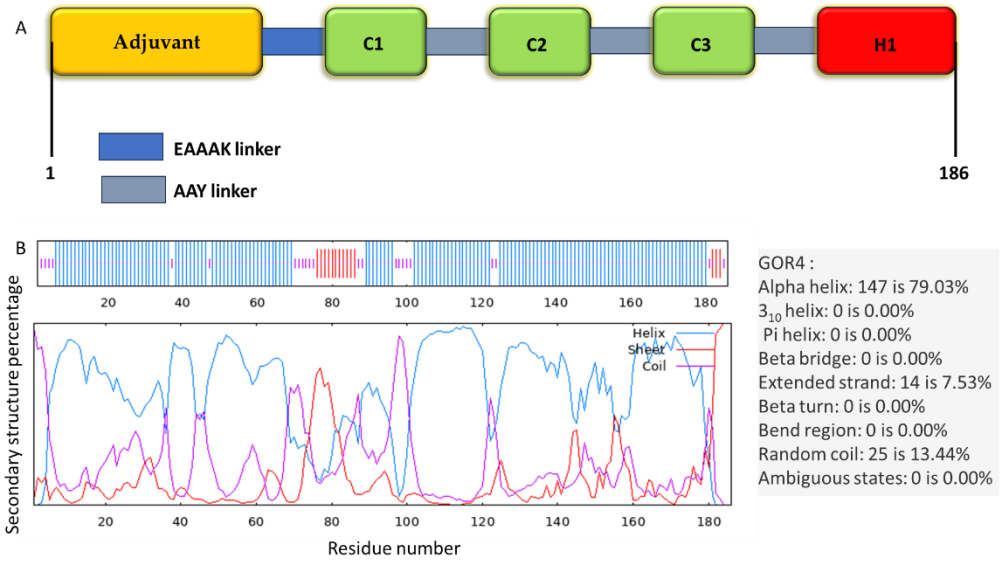

Figure 2. (A). The configuration of the final multi-epitope vaccine design. (B) The graphical representation of the secondary structure configuration of the constructed vaccine.

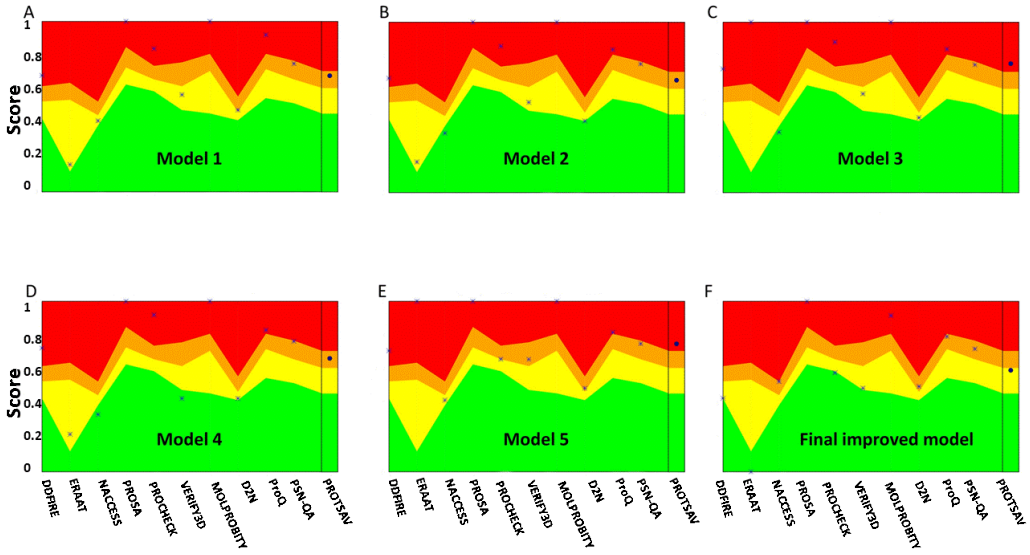

Figure 3. ProTSAV quality assessment of input vaccine models; (A) 1, (B) 2, (C) 3, (D) 4, (E) 5, and (F) further refined model. Green region indicates the input structure to be in 0–2 Å RMSD, yellow region 2–5 Å RMSD, orange region 5–8 Å RMSD and red region indicates structures beyond 8 Å RMSD. The

 doi:10.20944/preprints202408.2058.v1

blue colored asterisk symbol represents quality assessment score by individual module and blue colored round symbol represents overall score by ProTSAV.

3.5. Prediction of the B-Cell Epitope

Three linear B-cell epitopes (7-mer) including AKAQTTK, AAYQTTK, and MAAQTTK were predicted by the BCPREDS with a score of 2.675. The ElliPro server also predicted five discontinuous B-cell epitopes in the tertiary structure of the vaccine (Figure 4). The minimum and maximum scores for the predicted discontinuous B-cell epitopes were 0.539 and 0.826, respectively (Table 3).

Table 3. A list of discontinuous B-cell epitopes predicted by the ElliPro server.

Start	End	Peptide	Number of residues	Score
158	186	AYTTKRKWEAAAAYDMAAQTTKRKWEAAH	29	0.826
1	16	MAKLSTDELLDAFKEM	16	0.716
114	127	DEAKAKLEAAGATV	14	0.656
69	76	AAGDKKIG	8	0.602
153	156	KWEA	4	0.539

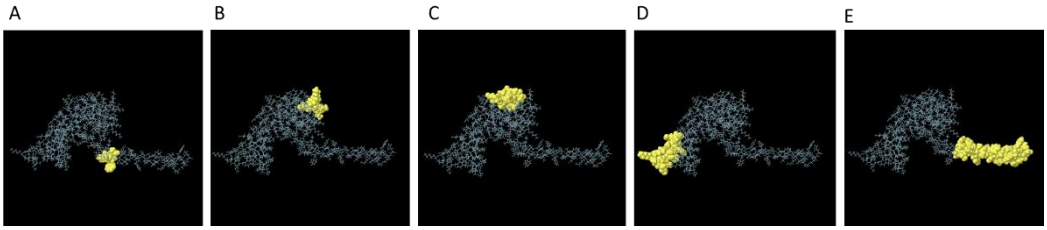

Figure 4. (A–E) 3D structure showing the discontinuous B-cell epitopes on the vaccine construct. The gray sticks and the yellow surface show the vaccine construct and discontinuous B-cell epitopes, respectively.

3.6. Predicted Interaction of the Vaccine Construct with TLR4

The molecular docking between the vaccine construct and TLR4 was accomplished using the ClusPro 2.0 server. In this study, the server produced 26 clusters and subsequently organized them based on their energy levels. The cluster with the most minimal energy, measuring at -1287.8, was selected as the optimal complex (Figure 5). Glu509 chain B and Lys560 chain A from TLR4 make salt-bridge with Lys 181 and Asp172 from vaccine construct, respectively. On the other hand, Asp580A, Lys560A, and Leu511B from TLR4 interact with Arg180, Ala169, and His186 from vaccine molecule via hydrogen bonds, respectively (Figure 5). As shown in Figure 5, TLR4 and vaccine construct interact with each other through π-cation interaction as well.

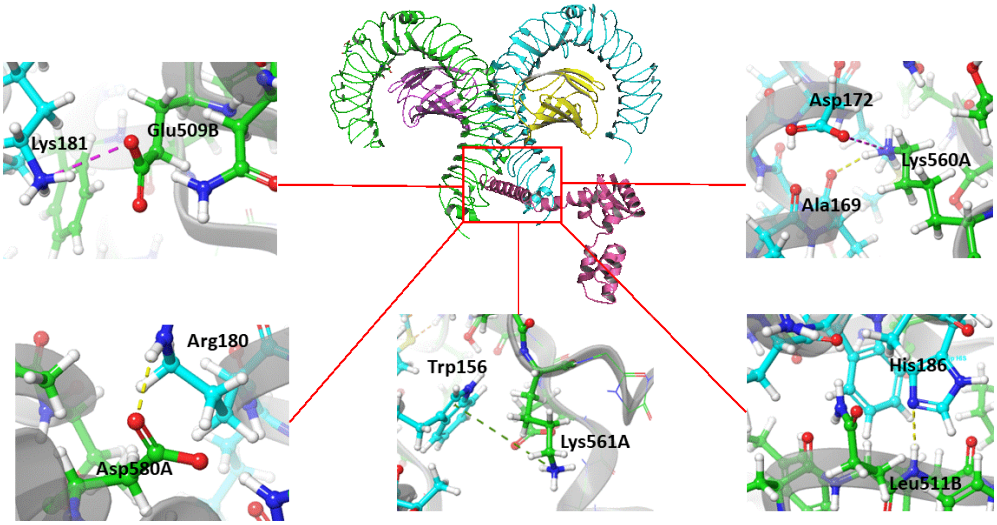

 doi:10.20944/preprints202408.2058.v1

Figure 5. Molecular docking of vaccine construct with TLR4 as an immune receptor. H-bonds, salt-bridge, and π-cation interactions are shown as yellow, purple and green dashed lines, respectively.

3.7. MD Simulation of Vaccine Construct with TLR4

The MD simulation spanned a robust 200 nanosecond timescale, during which we meticulously analyzed a variety of critical intermolecular interactions. We generated insightful plots for Root Mean Square Deviation (RMSD), Root Mean Square Fluctuation (RMSF), and Radius of gyration (Rg) to assess the dynamic flexibility and overall stability of the vaccine-receptor complex, as depicted in Figure 6. Our MD data provided valuable insights into the nature of interactions within the complex. Notably, hydrogen bonding emerged as the predominant non-covalent interaction between the vaccine construct and TLR4, exhibiting an average value of 13 H-bonds (Figure 6A). Meanwhile, the average count of salt-bridge interactions between the two proteins was determined to be 5.3, highlighting their significance in the binding process. In contrast, π-π stacking and π-cation interactions exhibited a comparatively minor contribution to the overall binding phenomenon.

The RMSD plot showed significant results highlighting the stability of the vaccine-TLR4 complex (Figure 6B). Our data unveiled that the vaccine exhibited greater flexibility relative to the TLR4 receptor. RMSF shows the movement and flexibility of each residue during the MD simulation. As depicted in Figure 6C, the regions of heightened flexibility were primarily concentrated at the loop area and the two termini of the vaccine. Furthermore, as the Rg value reflects the compactness of the complex structure, there should be fewer movements or deviation of the positions of the residues of the TLR4 or vaccine construct in the simulation trajectory in order to deem the complex to be stable. Remarkably, the Rg plot, as shown in Figure 6D, exhibited minimal deviation for both proteins throughout the course of the simulation. This consistency was visually represented by the relatively flat curve, a compelling testament to the compactness and enduring stability of the vaccine-TLR4 complex. Following the clustering of the MD trajectories, we conducted a comprehensive examination of the interactions between the vaccine and TLR4 residues, with the detailed findings presented in Table 4.

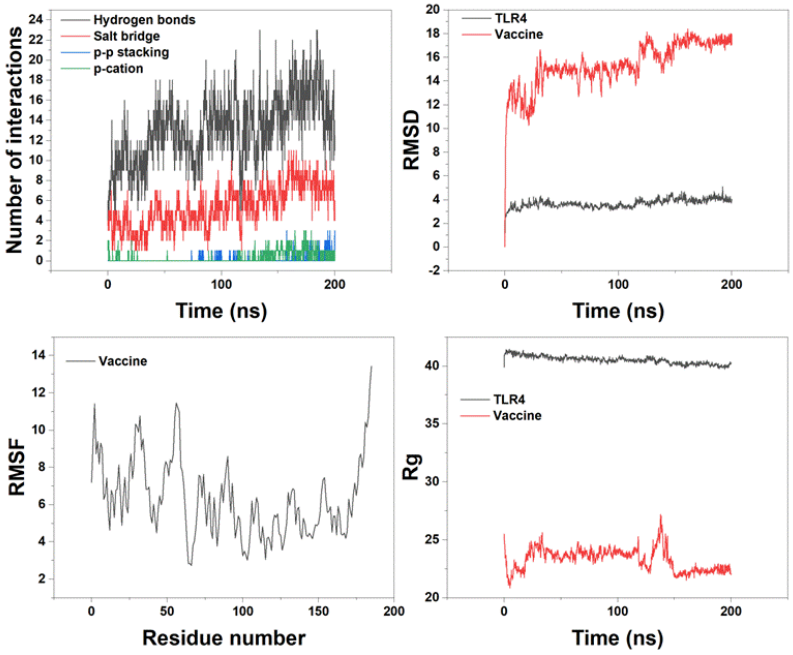

Figure 6. Molecular dynamics (MD) simulation trajectory plot of final vaccine construct with TLR4. (A) Number of interactions between the vaccine and TLR4. (B) Root Mean Square Deviation (RMSD) of vaccine and TLR4. (C) Root Mean Square Fluctuation (RMSF) of vaccine. (D) Radius of gyration (Rg) of vaccine and TLR4.

 doi:10.20944/preprints202408.2058.v1

In total, the analysis revealed the formation of eleven hydrogen bonds and three salt-bridges between the vaccine and the receptor (Table 4).

Table 4. The interaction between vaccine and TLR4 residues followed by cluster analysis during MD simulation.

Vaccine residue	TLR4 residue and chain	Distance(Å)	Type of interaction
Glu 183	Gln 616A	2.5	Hydrogen bond
Glu 183	Ser 613A	1.9	Hydrogen bond
Lys 181	Gln 510B	1.9	Hydrogen bond
Arg 180	Asp 580A	2.1	Hydrogen bond
Gln 176	Asp 580A	1.8	Hydrogen bond
Gln 176	His 555A	1.9	Hydrogen bond
Glu 166	Gln 616B	2.1	Hydrogen bond
Arg 163	Gln 616B	1.9	Hydrogen bond
Lys 151	Gly 617B	2.5	Hydrogen bond
Tyr 147	Ser 622B	1.9	Hydrogen bond
Lys 94	Glu 24B	2.2	Hydrogen bond
Lys 94	Glu 27B	2	Salt-bridge
Lys 91	Glu 24B	2.3	Salt-bridge
Lys 91	Glu 31B	2	Salt-bridge

3.8. Immune Simulation

The *in-silico* immune simulation using C-ImmSim for consecutive three injections given one month apart yielded outcomes congruent with real-world immune responses, as indicated by a significant augmentation in the production of secondary responses (Figure 7A-I). The primary immune response was distinguished by its notable abundance of immunoglobulin M (IgM). For each successive immunization (secondary and tertiary responses), there were conspicuous rises in antibody levels (comprising IgG1 + IgG2, IgM, and IgG + IgM) with a corresponding decline in antigen concentration as shown in Figure 7A and 7F. In our current investigation, we observed that the immune simulation for the vaccine demonstrated a substantial augmentation in the population of lymphocytes along with heightened production of IFN-γ and IL-2, as depicted in Figure 7B. Furthermore, the vaccine construct initiated the proliferation of B-cell populations following each successive injection (Figure 7C). Simulation results indicate the development of immune memory in the regions near the intermediate period (Figure 7D). Moreover, there was a pronounced heightened response observed in both the helper and cytotoxic T-cell populations, concomitant with the development of memory cells, as depicted in Figures 7D, 7E, 7G, and 7H. Following the administration of the vaccine, there was a notable increase in NK cell counts, and this heightened level was sustained throughout the simulation period (Figure 7I).

 doi:10.20944/preprints202408.2058.v1

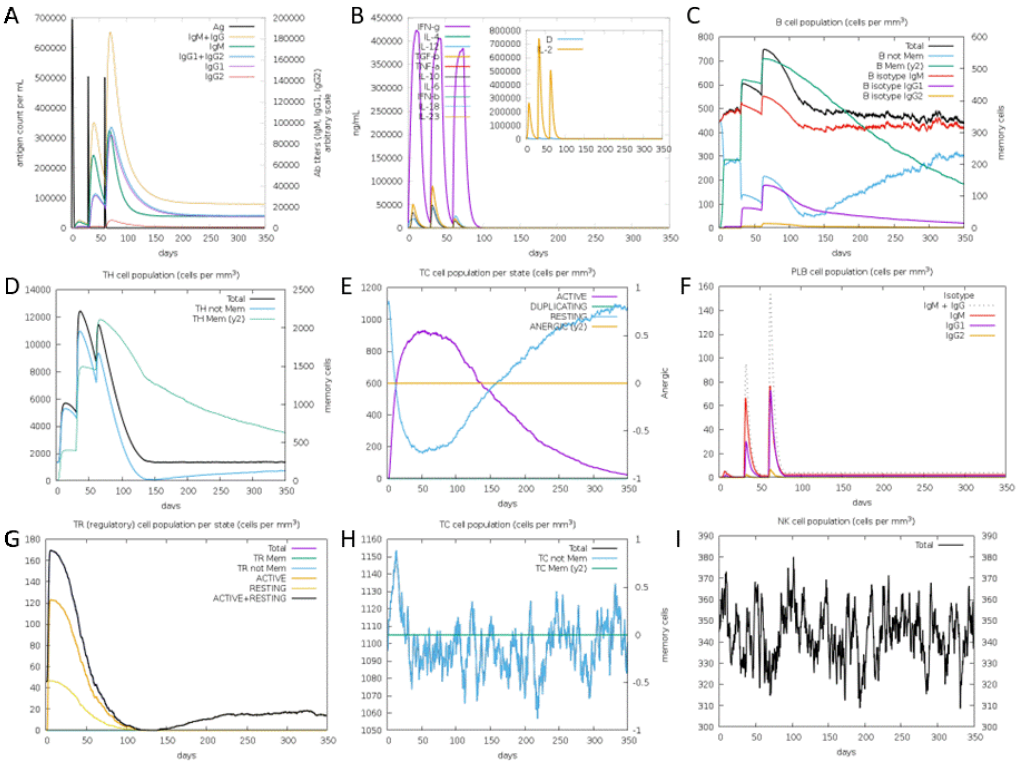

Figure 7. Predicted immune response following consecutive three injections of the final construct vaccine given one month apart. (A) The frequency of different Immunoglobulin and immunocomplexes production in response to antigen injections (black). Various subclasses are presented as colored peaks. (B) Various cytokine and interleukins. (C) The prediction of computed B-cell amounts. (D) The prediction of T-helper, (E) T-cytotoxic cell amounts per state, (F) various IgG subclasses, (G) CD4 T-regulatory lymphocytes count showing total/memory/per entity-state counts, (H) CD8 T-cytotoxic lymphocytes count showing total and memory populations, and (I) NK cell populations after three vaccine injections.

4. Discussion

GBM in adults stands out as one of the most lethal and challenging forms of malignant solid tumors. In the United States, approximately 12,120 patients were diagnosed with GBM in 2016, and they faced a daunting 5-year survival rate of only 5%. Despite extensive research endeavors, there has been minimal headway in extending the lifespan of GBM patients [4]. Hence, significant efforts are underway to explore novel approaches, including preventive and therapeutic GBM vaccines [54]. Various GBM vaccines, such as those based on Heat Shock Protein (HSP) and dendritic cells (DCs), have demonstrated efficacy in animal models but have not yet successfully transitioned into human clinical trials [54-56]. The emergence of advanced genomic sequencing technologies offers the potential for crafting individualized vaccines directed at specific neoantigens [57]. Neoantigens, arising from genetic mutations within cancer cells, can be identified as foreign antigens by the immune system [58]. Peptide-based cancer vaccines targeting neoantigens restrain the likelihood of tolerance as well as normal tissue toxicity and improve antitumor immune response compared with common cancer vaccines [57].

The current study focused on the development and *in-silico* design of a potential peptide-based vaccine for GBM using four neoantigens (PLAUR, ITGB3, HLA-B, and HLA-A) that are overexpressed in GBM compared to normal brain tissues. These proteins hold great promise as targets for vaccine development strategies, as any vaccine created could serve as potential preventive or therapeutic agents [20]. The surface proteins we chose showed promise as vaccine candidates in immunogenic investigations, as indicated by our bioinformatics analysis. In our study, we utilized the TCGA database to examine the gene expression profiles of our target proteins. Our analysis

 doi:10.20944/preprints202408.2058.v1

consistently revealed substantial overexpression of these proteins in GBM samples when compared to normal tissue. Additionally, we explored the correlation between the expression levels of these selected proteins and the survival of GBM patients using clinical data from the TCGA database. Our survival analysis unveiled a compelling trend: an increase in the gene expression of these proteins was associated with a notable decrease in the survival probability among GBM patients. These findings signify the potential clinical significance of these proteins in the context of GBM and provide a valuable foundation for vaccine design. In our epitope design process, we focused on the mutated segments within the neoantigens under investigation to craft both CTL and Th cell epitopes. This is essential to avoid targeting the wild-type proteins which could lead to further complications, as demonstrated by the involvement of platelets in immune responses generated against wild-type ITGB3, which can result in immune thrombocytopenia [59-61]. Subsequently, we rigorously evaluated these epitopes for their antigenic, allergenic, and toxic properties, along with their ability to induce IFN-γ and IL-4 responses. The resultant vaccine construct was assembled with meticulous care, consisting of three CTL epitopes, one Th cell epitope, along with the inclusion of an adjuvant, EAAAK, and AAY linker sequences. The employed linker sequences promote epitope presentation, while they also decrease the possibility of the formation of junctional epitopes [62]. The presence of the EAAAK linker serves to diminish the interaction with adjacent protein regions, thereby enhancing overall stability [63,64]. It has been demonstrated that the 50S ribosomal protein L7/L12, which we employed as an adjuvant, possesses an affinity for TLR4 [65-67].

The suggested vaccine construct demonstrated antigenicity while remaining non-allergenic, signifying its ability to effectively trigger strong immune responses without posing the risk of provoking harmful allergic reactions. The theoretical pI of the vaccine was found to be 5.7, indicating that the vaccine is acidic in nature. The molecular weight of the vaccine was 19.88 kDa, which is appropriate since proteins with molecular weights less than 110 kDa are easier and quicker to purify [68]. The vaccine exhibited a substantial proportion of α-helical structure (79.03%), resulting in a calculated instability index of 24.96. This value falls below the threshold of 40, signifying that the vaccine can be classified as a stable protein [32]. In 2021, Gharbavi et al. designed a vaccine construct from three proteins: IL-13Rα2, TNC, and PTPRZ-1 [69]. The half-life of our vaccine was determined to be 30 h in mammalian reticulocytes, while the half-life of the constructs designed in the study of Gharbavi et al. was 1.1 hour [69], indicating that our vaccine would be exposed to the immune system for a longer period of time than the vaccines designed by Gharbavi et al. The aliphatic index of the vaccine was calculated to be 81.67, which is higher than vaccine designed by Gharbavi et al. [69], Sanami et al. [70], and Kumar et al. [71], and shows that our vaccine is thermostable.

Upon constructing the three-dimensional structure of the vaccine, we employed a refinement process to enhance its quality, bringing it closer to its native conformation. We conducted a thorough assessment of the model's quality, confirming the high quality and reliability of our vaccine model. It has been found that TLR4 is expressed at least in 43% of GBM cells in the xenograft [69]. TLR4 exhibits anti-tumor effects that operate independently of the presence of active immune cells [72]. Hence, we conducted molecular docking analysis to examine the interaction between the vaccine and TLR4. The molecular docking analysis revealed a strong interaction between the vaccine and TLR4. Subsequently, we subjected the docked vaccine-TLR4 complex to MD simulation to assess the stability of the vaccine construct. Our MD data clearly demonstrated that hydrogen bonding stands out as the pivotal interaction between the vaccine and TLR4. The RMSD plot, which was generated for the proposed vaccine and TLR4, indicated the stability of both entities. Furthermore, the RMSF analysis unveiled that the vaccine construct exhibited minimal fluctuations, particularly in regions characterized by extensive interactions with TLR4.

It has been well documented that immunity against GBM relies on the concerted action of both B and T lymphocytes [73,74]. While the involvement of cytotoxic T cells in eliminating peripheral and brain tumors has been extensively studied and confirmed [75,76], research has also underscored the significant contribution of B cells in augmenting the costimulatory signaling between dendritic cells (DCs) and T cells [77]. According to our findings, the concentrations of IFN-γ and IL-2 exhibited an initial increase after the initial injection and consistently maintained their peak levels with subsequent

 doi:10.20944/preprints202408.2058.v1

exposures to the antigen. This observation suggests the presence of elevated T-helper cell (THC) activity, leading to an efficient production of immunoglobulins and endorsing a humoral immune response. The immune simulation yielded outcomes in alignment with conventional immune responses, demonstrating a general augmentation in immune responses with repeated exposure to the antigen. In the context of GBM, it is worth noting that IgG, IgM, and IgA responses to glioma antigens are implicated in disease protection [78-80].

Since *in-silico* approaches have inherent limitations when it comes to predicting physicochemical properties, structural aspects, and immunogenicity, the effectiveness of our proposed vaccine must be substantiated through additional laboratory experiments.

5. Conclusions

Finding effective solutions for GBM treatment in a clinical setting remains a formidable challenge, necessitating the development of innovative approaches. No proper treatments are available for the patients yet. The emergence of immunotherapy presents a potential avenue for effective treatment, and the utilization of *in-silico* methods could prove advantageous in designing a potent vaccine against this devastating disease. In this study, we harnessed immuno-informatic tools and an MD approach to formulate a multi-epitope peptide vaccine targeting GBM. This vaccine was meticulously crafted based on overexpressed cell surface neoantigens found on GBM cells. Our designed vaccine exhibited the capacity to elicit a robust immune response, as evidenced by computer-based predictions of its immunogenicity and antigenicity. Our proposed vaccine holds the potential to serve as a supplementary tool aimed at enhancing treatment outcomes for GBM. The proposed vaccine needs future both in vitro and in vivo studies.

Supplementary Materials: The following supporting information can be downloaded at the website of this paper posted on Preprints.org, Figure S1: Expression profile and survival probability of target gene in normal and GBM cancer patients. Data were curated from ULCAN and TCGA database. Expression profile (A) and survival probability (B) of HLA-B; Expression profile (C) and survival probability (D) of PLAUR; Expression profile (E) and survival probability (F) of HLA-A; Expression profile (G) and survival probability (H) of ITGB3, Figure S2: Computed interaction between epitope C1 and HLA-A1 by molecular docking, Figure S3. Computed interaction between epitope C2 and HLA-A1 by molecular docking, Figure S4: Computed interaction between epitope C3 and HLA-A1 by molecular docking, Figure S5: Computed interaction between epitope C1 and HLA-A2 by molecular docking, Figure S6: Computed interaction between epitope C2 and HLA-A2 by molecular docking, Figure S7: Computed interaction between epitope C3 and HLA-A2 by molecular docking, Figure S8: Computed interaction between epitope C1 and HLA-A3 by molecular docking, Figure S9: Computed interaction between epitope C2 and HLA-A3 by molecular docking, Figure S10: Computed interaction between epitope C3 and HLA-A3 by molecular docking.

Author Contributions: Conceptualization, S.M. and X.Y.W.; methodology, S.M.; writing—original draft preparation, S.M., K.D.Y, X.Y.W. and H.N.; writing—review and editing, S.M., K.D.Y, X.Y.W. and H.N; supervision, X.Y.W.; All authors have read and agreed to the published version of the manuscript.

Funding: This work was supported in part by the Natural Sciences and Engineering Research Council (NSERC) of Canada Discovery Grant to XYW.

Institutional Review Board Statement: Not applicable.

Informed Consent Statement: Not applicable.

Data Availability Statement: The PDB ID for TLR4 is 4G8A, which can be downloaded from the Protein Data Bank (https://www.rcsb.org/). The wild-type amino acid sequences of four surface proteins—PLAUR (Q03405), ITGB3 (P05106), HLA-B (P01889), and HLA-A (P04439)—are available for download from the UniProt database (https://www.uniprot.org/).

Acknowledgments: NSERC CREATE ContRoL scholarship, Mitacs Accelerate Internship, Pfizer Canada Graduate Fellowship in Pharmaceutical Sciences, and Department of Pharmaceutical Sciences Top-Up scholarship to S.M.

Conflicts of Interest: The authors declare no conflict of interest.

References

 doi:10.20944/preprints202408.2058.v1

1. Louis, D.N.; Perry, A.; Reifenberger, G.; Von Deimling, A.; Figarella-Branger, D.; Cavenee, W.K.; Ohgaki, H.; Wiestler, O.D.; Kleihues, P.; Ellison, D.W. The 2016 World Health Organization classification of tumors of the central nervous system: a summary. *Acta neuropathologica* **2016**, *131*, 803-820.
2. Ostrom, Q.T.; Cioffi, G.; Gittleman, H.; Patil, N.; Waite, K.; Kruchko, C.; Barnholtz-Sloan, J.S. CBTRUS statistical report: primary brain and other central nervous system tumors diagnosed in the United States in 2012–2016. *Neuro-oncology* **2019**, *21*, v1-v100.
3. Ostrom, Q.T.; Gittleman, H.; Fulop, J.; Liu, M.; Blanda, R.; Kromer, C.; Wolinsky, Y.; Kruchko, C.; Barnholtz-Sloan, J.S. CBTRUS statistical report: primary brain and central nervous system tumors diagnosed in the United States in 2008-2012. *Neuro-oncology* **2015**, *17*, iv1-iv62.
4. Alexander, B.M.; Cloughesy, T.F. Adult glioblastoma. *Journal of Clinical Oncology* **2017**, *35*, 2402-2409.
5. Hanahan, D.; Weinberg, R.A. Hallmarks of cancer: the next generation. *cell* **2011**, *144*, 646-674.
6. Stupp, R.; Hegi, M.E.; Mason, W.P.; Van Den Bent, M.J.; Taphoorn, M.J.; Janzer, R.C.; Ludwin, S.K.; Allgeier, A.; Fisher, B.; Belanger, K. Effects of radiotherapy with concomitant and adjuvant temozolomide versus radiotherapy alone on survival in glioblastoma in a randomised phase III study: 5-year analysis of the EORTC-NCIC trial. *The lancet oncology* **2009**, *10*, 459-466.
7. Frosina, G. Limited advances in therapy of glioblastoma trigger re-consideration of research policy. *Critical reviews in oncology/hematology* **2015**, *96*, 257-261.
8. Cao, J.-X.; Zhang, X.-Y.; Liu, J.-L.; Li, D.; Li, J.-L.; Liu, Y.-S.; Wang, M.; Xu, B.-L.; Wang, H.-B.; Wang, Z.-X. Clinical efficacy of tumor antigen-pulsed DC treatment for high-grade glioma patients: evidence from a meta-analysis. *PloS one* **2014**, *9*, e107173.
9. Maxwell, R.; Jackson, C.M.; Lim, M. Clinical trials investigating immune checkpoint blockade in glioblastoma. *Current treatment options in oncology* **2017**, *18*, 1-22.
10. Kaneko, M.K.; Kunita, A.; Abe, S.; Tsujimoto, Y.; Fukayama, M.; Goto, K.; Sawa, Y.; Nishioka, Y.; Kato, Y. Chimeric anti-podoplanin antibody suppresses tumor metastasis through neutralization and antibody-dependent cellular cytotoxicity. *Cancer science* **2012**, *103*, 1913-1919.
11. Kumai, T.; Fan, A.; Harabuchi, Y.; Celis, E. Cancer immunotherapy: moving forward with peptide T cell vaccines. *Current opinion in immunology* **2017**, *47*, 57-63.
12. Okada, H.; Kalinski, P.; Ueda, R.; Hoji, A.; Kohanbash, G.; Donegan, T.E.; Mintz, A.H.; Engh, J.A.; Bartlett, D.L.; Brown, C.K. Induction of CD8+ T-cell responses against novel glioma–associated antigen peptides and clinical activity by vaccinations with α-type 1 polarized dendritic cells and polyinosinic-polycytidylic acid stabilized by lysine and carboxymethylcellulose in patients with recurrent malignant glioma. *Journal of clinical oncology* **2011**, *29*, 330.
13. Saleh, M.; Davis, I.D.; Wilks, A.F. The paracrine role of tumour-derived mIL-4 on tumour-associated endothelium. *International journal of cancer* **1997**, *72*, 664-672.
14. Gadani, S.P.; Cronk, J.C.; Norris, G.T.; Kipnis, J. IL-4 in the brain: a cytokine to remember. *The journal of immunology* **2012**, *189*, 4213-4219.
15. Carlsson, A.; Persson, O.; Ingvarsson, J.; Widegren, B.; Salford, L.; Borrebaeck, C.A.; Wingren, C. Plasma proteome profiling reveals biomarker patterns associated with prognosis and therapy selection in glioblastoma multiforme patients. *PROTEOMICS–Clinical Applications* **2010**, *4*, 591-602.
16. Ferrandez, E.; Gutierrez, O.; Segundo, D.S.; Fernandez-Luna, J.L. NFκB activation in differentiating glioblastoma stem-like cells is promoted by hyaluronic acid signaling through TLR4. *Scientific Reports* **2018**, *8*, 6341.
17. Brennan, C.W.; Verhaak, R.G.; McKenna, A.; Campos, B.; Noushmehr, H.; Salama, S.R.; Zheng, S.; Chakravarty, D.; Sanborn, J.Z.; Berman, S.H. The somatic genomic landscape of glioblastoma. *Cell* **2013**, *155*, 462-477.
18. Schumacher, T.; Bunse, L.; Pusch, S.; Sahm, F.; Wiestler, B.; Quandt, J.; Menn, O.; Osswald, M.; Oezen, I.; Ott, M. A vaccine targeting mutant IDH1 induces antitumour immunity. *Nature* **2014**, *512*, 324-327.
19. Weller, M.; Butowski, N.; Tran, D.; Recht, L.; Lim, M.; Hirte, H.; Ashby, L.; Mechtler, L.; Goldlust, S.; Iwamoto, F. ATIM-03. ACT IV: an international, double-blind, phase 3 trial of rindopepimut in newly diagnosed, EGFRvIII-expressing glioblastoma. **2016**.
20. Rose, M.; Cardon, T.; Aboulouard, S.; Hajjaji, N.; Kobeissy, F.; Duhamel, M.; Fournier, I.; Salzet, M. Surfaceome proteomic of glioblastoma revealed potential targets for immunotherapy. *Frontiers in Immunology* **2021**, *12*, 746168.
21. Zhai, B.-T.; Tian, H.; Sun, J.; Zou, J.-B.; Zhang, X.-F.; Cheng, J.-X.; Shi, Y.-J.; Fan, Y.; Guo, D.-Y. Urokinase-type plasminogen activator receptor (uPAR) as a therapeutic target in cancer. *Journal of Translational Medicine* **2022**, *20*, 135.
22. Echavidre, W.; Picco, V.; Faraggi, M.; Montemagno, C. Integrin-αvβ3 as a Therapeutic Target in Glioblastoma: Back to the Future? *Pharmaceutics* **2022**, *14*, 1053.
23. Shraibman, B.; Barnea, E.; Kadosh, D.M.; Haimovich, Y.; Slobodin, G.; Rosner, I.; López-Larrea, C.; Hilf, N.; Kuttruff, S.; Song, C. Identification of tumor antigens among the HLA peptidomes of glioblastoma tumors and plasma. *Molecular & Cellular Proteomics* **2018**, *17*, 2132-2145.

24. Consortium, U. Reorganizing the protein space at the Universal Protein Resource (UniProt). *Nucleic acids research* **2012**, *40*, D71-D75.
25. Chandrashekar, D.S.; Karthikeyan, S.K.; Korla, P.K.; Patel, H.; Shovon, A.R.; Athar, M.; Netto, G.J.; Qin, Z.S.; Kumar, S.; Manne, U. UALCAN: An update to the integrated cancer data analysis platform. *Neoplasia* **2022**, *25*, 18-27.
26. Doytchinova, I.A.; Flower, D.R. VaxiJen: a server for prediction of protective antigens, tumour antigens and subunit vaccines. *BMC bioinformatics* **2007**, *8*, 1-7.
27. Dimitrov, I.; Bangov, I.; Flower, D.R.; Doytchinova, I. AllerTOP v. 2—a server for in silico prediction of allergens. *Journal of molecular modeling* **2014**, *20*, 1-6.
28. Wold, S.; Jonsson, J.; Sjörström, M.; Sandberg, M.; Rännar, S. DNA and peptide sequences and chemical processes multivariately modelled by principal component analysis and partial least-squares projections to latent structures. *Analytica Chimica Acta* **1993**, *277*, 239-253.
29. Dhanda, S.K.; Gupta, S.; Vir, P.; Raghava, G. Prediction of IL4 inducing peptides. *Clinical and Developmental Immunology* **2013**, *2013*.
30. Dhanda, S.K.; Vir, P.; Raghava, G.P. Designing of interferon-gamma inducing MHC class-II binders. *Biology direct* **2013**, *8*, 1-15.
31. Magnan, C.N.; Zeller, M.; Kayala, M.A.; Vigil, A.; Randall, A.; Felgner, P.L.; Baldi, P. High-throughput prediction of protein antigenicity using protein microarray data. *Bioinformatics* **2010**, *26*, 2936-2943.
32. Gasteiger, E.; Hoogland, C.; Gattiker, A.; Duvaud, S.e.; Wilkins, M.R.; Appel, R.D.; Bairoch, A. *Protein identification and analysis tools on the ExPASy server*; Springer: 2005.
33. Garnier, J. GOR secondary structure prediction method version IV. *Meth. Enzym., RF Doolittle Ed.* **1998**, *266*, 540-553.
34. Roy, A.; Kucukural, A.; Zhang, Y. I-TASSER: a unified platform for automated protein structure and function prediction. *Nature protocols* **2010**, *5*, 725-738.
35. Singh, A.; Kaushik, R.; Mishra, A.; Shanker, A.; Jayaram, B. ProTSAV: A protein tertiary structure analysis and validation server. *Biochimica et Biophysica Acta (BBA)-Proteins and Proteomics* **2016**, *1864*, 11-19.
36. Lee, G.R.; Won, J.; Heo, L.; Seok, C. GalaxyRefine2: simultaneous refinement of inaccurate local regions and overall protein structure. *Nucleic acids research* **2019**, *47*, W451-W455.
37. Khan, M.; Khan, S.; Ali, A.; Akbar, H.; Sayaf, A.M.; Khan, A.; Wei, D.-Q. Immunoinformatics approaches to explore Helicobacter Pylori proteome (Virulence Factors) to design B and T cell multi-epitope subunit vaccine. *Scientific reports* **2019**, *9*, 13321.
38. Saha, S.; Raghava, G.P.S. BcePred: prediction of continuous B-cell epitopes in antigenic sequences using physico-chemical properties. In Proceedings of the International conference on artificial immune systems, 2004; pp. 197-204.
39. Chen, J.; Liu, H.; Yang, J.; Chou, K.-C. Prediction of linear B-cell epitopes using amino acid pair antigenicity scale. *Amino acids* **2007**, *33*, 423-428.
40. Ponomarenko, J.; Bui, H.-H.; Li, W.; Fusseder, N.; Bourne, P.E.; Sette, A.; Peters, B. ElliPro: a new structure-based tool for the prediction of antibody epitopes. *BMC bioinformatics* **2008**, *9*, 1-8.
41. Laxmi, D.; Priyadarshy, S. HyperChem 6.03. *Biotech Software & Internet Report: The Computer Software Journal for Scientists* **2002**, *3*, 5-9.
42. Trott, O.; Olson, A.J. AutoDock Vina: improving the speed and accuracy of docking with a new scoring function, efficient optimization, and multithreading. *Journal of computational chemistry* **2010**, *31*, 455-461.
43. Ohto, U.; Yamakawa, N.; Akashi-Takamura, S.; Miyake, K.; Shimizu, T. Structural analyses of human Toll-like receptor 4 polymorphisms D299G and T399I. *Journal of Biological Chemistry* **2012**, *287*, 40611-40617.
44. Desta, I.T.; Porter, K.A.; Xia, B.; Kozakov, D.; Vajda, S. Performance and its limits in rigid body protein-protein docking. *Structure* **2020**, *28*, 1071-1081. e1073.
45. Release, S. 3: Desmond molecular dynamics system, DE Shaw research, New York, NY, 2017. *Maestro-Desmond Interoperability Tools, Schrödinger, New York, NY* **2017**.
46. Banks, J.L.; Beard, H.S.; Cao, Y.; Cho, A.E.; Damm, W.; Farid, R.; Felts, A.K.; Halgren, T.A.; Mainz, D.T.; Maple, J.R. Integrated modeling program, applied chemical theory (IMPACT). *Journal of computational chemistry* **2005**, *26*, 1752-1780.
47. Toukmaji, A.Y.; Board Jr, J.A. Ewald summation techniques in perspective: a survey. *Computer physics communications* **1996**, *95*, 73-92.
48. Mark, P.; Nilsson, L. Structure and dynamics of the TIP3P, SPC, and SPC/E water models at 298 K. *The Journal of Physical Chemistry A* **2001**, *105*, 9954-9960.
49. Martyna, G.J.; Tuckerman, M.E.; Tobias, D.J.; Klein, M.L. Explicit reversible integrators for extended systems dynamics. *Molecular Physics* **1996**, *87*, 1117-1157.
50. Martyna, G.J.; Klein, M.L.; Tuckerman, M. Nosé–Hoover chains: The canonical ensemble via continuous dynamics. *The Journal of chemical physics* **1992**, *97*, 2635-2643.
51. Humphrey, W.; Dalke, A.; Schulten, K. VMD: visual molecular dynamics. *Journal of molecular graphics* **1996**, *14*, 33-38.

 doi:10.20944/preprints202408.2058.v1

52. Rapin, N.; Lund, O.; Bernaschi, M.; Castiglione, F. Computational immunology meets bioinformatics: the use of prediction tools for molecular binding in the simulation of the immune system. *PloS one* **2010**, *5*, e9862.
53. Ikai, A. Thermostability and aliphatic index of globular proteins. *The Journal of Biochemistry* **1980**, *88*, 1895-1898.
54. Dey, M.; Chang, A.L.; Miska, J.; Wainwright, D.A.; Ahmed, A.U.; Balyasnikova, I.V.; Pytel, P.; Han, Y.; Tobias, A.; Zhang, L. Dendritic cell–based vaccines that utilize myeloid rather than plasmacytoid cells offer a superior survival advantage in malignant glioma. *The Journal of Immunology* **2015**, *195*, 367-376.
55. Iglesia, R.P.; Fernandes, C.F.d.L.; Coelho, B.P.; Prado, M.B.; Melo Escobar, M.I.; Almeida, G.H.D.R.; Lopes, M.H. Heat shock proteins in glioblastoma biology: where do we stand? *International Journal of Molecular Sciences* **2019**, *20*, 5794.
56. Yang, I.; Han, S.; Parsa, A.T. Heat-shock protein vaccines as active immunotherapy against human gliomas. *Expert review of anticancer therapy* **2009**, *9*, 1577-1582.
57. Liu, J.; Miao, L.; Sui, J.; Hao, Y.; Huang, G. Nanoparticle cancer vaccines: Design considerations and recent advances. *Asian Journal of Pharmaceutical Sciences* **2020**, *15*, 576-590.
58. Kiyotani, K.; Chan, H.T.; Nakamura, Y. Immunopharmacogenomics towards personalized cancer immunotherapy targeting neoantigens. *Cancer Science* **2018**, *109*, 542-549.
59. Yougbare, I.; Lang, S.; Yang, H.; Chen, P.; Zhao, X.; Tai, W.-S.; Zdravic, D.; Vadasz, B.; Li, C.; Piran, S. Maternal anti-platelet β3 integrins impair angiogenesis and cause intracranial hemorrhage. *The Journal of clinical investigation* **2015**, *125*, 1545-1556.
60. Li, J.; Sullivan, J.A.; Ni, H. Pathophysiology of immune thrombocytopenia. *Current opinion in hematology* **2018**, *25*, 373-381.
61. Ni, H.; Freedman, J. Platelets in hemostasis and thrombosis: role of integrins and their ligands. *Transfusion and Apheresis Science* **2003**, *28*, 257-264.
62. Nezafat, N.; Karimi, Z.; Eslami, M.; Mohkam, M.; Zandian, S.; Ghasemi, Y. Designing an efficient multi-epitope peptide vaccine against Vibrio cholerae via combined immunoinformatics and protein interaction based approaches. *Computational biology and chemistry* **2016**, *62*, 82-95.
63. Arai, R.; Ueda, H.; Kitayama, A.; Kamiya, N.; Nagamune, T. Design of the linkers which effectively separate domains of a bifunctional fusion protein. *Protein engineering* **2001**, *14*, 529-532.
64. Pandey, R.K.; Narula, A.; Naskar, M.; Srivastava, S.; Verma, P.; Malik, R.; Shah, P.; Prajapati, V.K. Exploring dual inhibitory role of febrifugine analogues against Plasmodium utilizing structure-based virtual screening and molecular dynamic simulation. *Journal of Biomolecular Structure and Dynamics* **2017**, *35*, 791-804.
65. Deng, H.; Yu, S.; Guo, Y.; Gu, L.; Wang, G.; Ren, Z.; Li, Y.; Li, K.; Li, R. Development of a multivalent enterovirus subunit vaccine based on immunoinformatic design principles for the prevention of HFMD. *Vaccine* **2020**, *38*, 3671-3681.
66. Pandey, R.K.; Prajapati, V.K. Exploring sand fly salivary proteins to design multiepitope subunit vaccine to fight against visceral leishmaniasis. *Journal of cellular biochemistry* **2019**, *120*, 1141-1155.
67. Chatterjee, N.; Ojha, R.; Khatoon, N.; Prajapati, V.K. Scrutinizing Mycobacterium tuberculosis membrane and secretory proteins to formulate multiepitope subunit vaccine against pulmonary tuberculosis by utilizing immunoinformatic approaches. *International journal of biological macromolecules* **2018**, *118*, 180-188.
68. Barh, D.; Barve, N.; Gupta, K.; Chandra, S.; Jain, N.; Tiwari, S.; Leon-Sicairos, N.; Canizalez-Roman, A.; Rodrigues dos Santos, A.; Hassan, S.S. Exoproteome and secretome derived broad spectrum novel drug and vaccine candidates in Vibrio cholerae targeted by Piper betel derived compounds. *PloS one* **2013**, *8*, e52773.
69. Gharbavi, M.; Danafar, H.; Amani, J.; Sharafi, A. Immuno-informatics analysis and expression of a novel multi-domain antigen as a vaccine candidate against glioblastoma. *International immunopharmacology* **2021**, *91*, 107265.
70. Sanami, S.; Azadegan-Dehkordi, F.; Rafieian-Kopaei, M.; Salehi, M.; Ghasemi-Dehnoo, M.; Mahooti, M.; Alizadeh, M.; Bagheri, N. Design of a multi-epitope vaccine against cervical cancer using immunoinformatics approaches. *Scientific Reports* **2021**, *11*, 12397.
71. Kumar, S.; Shuaib, M.; Prajapati, K.S.; Singh, A.K.; Choudhary, P.; Singh, S.; Gupta, S. A candidate triple-negative breast cancer vaccine design by targeting clinically relevant cell surface markers: an integrated immuno and bio-informatics approach. *3 Biotech* **2022**, *12*, 72.
72. Finocchiaro, G. TLRgeting evasion of immune pathways in glioblastoma. *Cell Stem Cell* **2017**, *20*, 422-424.
73. Candolfi, M.; Curtin, J.F.; Yagiz, K.; Assi, H.; Wibowo, M.K.; Alzadeh, G.E.; Foulad, D.; Muhammad, A.G.; Salehi, S.; Keech, N. B cells are critical to T-cell—mediated antitumor immunity induced by a combined immune-stimulatory/conditionally cytotoxic therapy for glioblastoma. *Neoplasia* **2011**, *13*, 947-IN923.
74. Pucci, F. Location-dependent B-cell function in glioblastoma. *Cancer Immunology Research* **2019**, *7*, 1902-1902.

 doi:10.20944/preprints202408.2058.v1

75. Wiencke, J.K.; Accomando, W.P.; Zheng, S.; Patoka, J.; Dou, X.; Phillips, J.J.; Hsuang, G.; Christensen, B.C.; Houseman, E.A.; Koestler, D.C. Epigenetic biomarkers of T-cells in human glioma. *Epigenetics* **2012**, *7*, 1391-1402.
76. Woroniecka, K.; Fecci, P.E. T-cell exhaustion in glioblastoma. *Oncotarget* **2018**, *9*, 35287.
77. Crawford, A.; MacLeod, M.; Schumacher, T.; Corlett, L.; Gray, D. Primary T cell expansion and differentiation in vivo requires antigen presentation by B cells. *The Journal of Immunology* **2006**, *176*, 3498-3506.
78. Oji, Y.; Hashimoto, N.; Tsuboi, A.; Murakami, Y.; Iwai, M.; Kagawa, N.; Chiba, Y.; Izumoto, S.; Elisseeva, O.; Ichinohasama, R. Association of WT1 IgG antibody against WT1 peptide with prolonged survival in glioblastoma multiforme patients vaccinated with WT1 peptide. *International journal of cancer* **2016**, *139*, 1391-1401.
79. Busch, S.; Talamini, M.; Brenner, S.; Abdulazim, A.; Hänggi, D.; Neumaier, M.; Seiz-Rosenhagen, M.; Fuchs, T. Circulating monocytes and tumor-associated macrophages express recombined immunoglobulins in glioblastoma patients. *Clinical and translational medicine* **2019**, *8*, 1-14.
80. Turki, S.G. Immunoglobulins Levels and Complements in Patients with Brain Tumour (Meningioma and Glioma). *Iraqi National Journal of Nursing Specialties* **2017**, *30*.